

Communication

Influence of Stratospheric Ozone Changes on Stratospheric Temperature Trends in Recent Decades

Lingyu Zhou ¹, Yan Xia ^{1,2,3,*}  and Chuanfeng Zhao ⁴ 

¹ College of Global Change and Earth System Science, Beijing Normal University, Beijing 100875, China

² School of Systems Science, Beijing Normal University, Beijing 100875, China

³ Key Laboratory of Middle Atmosphere and Global Environment Observation, Institute of Atmospheric Physics, Chinese Academy of Sciences, Beijing 100029, China

⁴ Laboratory for Climate and Ocean-Atmosphere Studies, Department of Atmospheric and Oceanic Sciences, School of Physics, Peking University, Beijing 100871, China

* Correspondence: xiayan@bnu.edu.cn

Abstract: Associated with the recovery of stratospheric ozone, stratospheric cooling has decelerated since the late 1990s. This study investigates the contribution of ozone changes to the long-term stratospheric temperature trends in recent decades using satellite observations and model simulations. Observational analysis shows that total column ozone experienced little depletion in the Northern Hemisphere (NH) and weak recovery in the Southern Hemisphere (SH) in the period 1998–2020. It is found that the cease of stratospheric ozone depletion has reduced the stratospheric cooling from 1998 onwards, especially in the summer hemisphere. The correlation analysis indicates that the lower-stratospheric temperature is primarily regulated by ozone changes. The ozone recovery in the SH is associated with the weak warming in the lower stratosphere in the period 1998–2020 in summer. The impact of ozone changes is further isolated in the ozone-only experiments from CMIP6. We find that ozone depletion results in significant cooling in the summer hemisphere in the period 1979–1997, especially in the upper and lower stratosphere, while ozone recovery leads to significant warming in the summer hemisphere in the period 1998–2020 in the upper stratosphere. Our results also suggest that the wave-mean flow interactions associated with stratospheric ozone variations may play an important role in regulating the strength of polar vortex in winter.

Keywords: stratospheric ozone; stratospheric temperature; long-term trends; satellite observations; CMIP6



Citation: Zhou, L.; Xia, Y.; Zhao, C. Influence of Stratospheric Ozone Changes on Stratospheric Temperature Trends in Recent Decades. *Remote Sens.* **2022**, *14*, 5364. <https://doi.org/10.3390/rs14215364>

Academic Editor: Manuel Antón

Received: 14 September 2022

Accepted: 20 October 2022

Published: 26 October 2022

Publisher's Note: MDPI stays neutral with regard to jurisdictional claims in published maps and institutional affiliations.



Copyright: © 2022 by the authors. Licensee MDPI, Basel, Switzerland. This article is an open access article distributed under the terms and conditions of the Creative Commons Attribution (CC BY) license (<https://creativecommons.org/licenses/by/4.0/>).

1. Introduction

One major focus of climatic research has been the impact of ozone depletion on stratospheric climate since the discovery of the Antarctic ozone hole in 1985 [1]. Previous studies suggest that the Antarctic ozone hole started in the late 1970s, which was driven by anthropogenic emissions of chlorofluorocarbons and brominated carbons [2–4]. In addition, relatively weak but significant ozone loss has been observed in the Arctic in boreal spring [5]. Stratospheric ozone experienced long-term depletion in the last several decades of the 20th century, especially in the upper stratosphere and in the two polar regions [2]. The long-term depletion of the ozone layer has become a major global scientific and environmental issue. This environmental issue has been significantly mitigated since the late 1990s as a result of the global phase-out of the long-lived ozone-depleting substances (ODSs) following the Montreal Protocol [6]. Both observations and model simulations suggest that the Antarctic ozone hole is beginning to slowly heal and recover [7], and that the ozone recovery in the upper stratosphere is also particularly evident in the last two decades [8]. The changes in stratospheric ozone are found to have pronounced climate effects on the tropospheric and surface climate [9–14]. The climatic responses to ozone depletion are expected to be reversed in the 21st century under ozone recovery [3,15–19].

Ozone-induced radiative effects are an important factor influencing the long-term trends of stratospheric temperature [20–23]. The observed stratospheric cooling in the last several decades is mainly driven by an increase in well-mixed greenhouse gases (GHGs) and a reduction in stratospheric ozone [24–26]. Observations show a strong cooling of about 1–3 K in the stratosphere over the past four decades (1979–2018) [27]. The strong cooling in the Antarctic lower stratosphere in summer was found to be caused by the radiative effects of severe ozone depletion [28,29], which has pronounced impacts on the tropospheric climate in the Southern Hemisphere [3,30,31]. A recent study indicates that a decrease in ozone in the upper troposphere and lower stratosphere (UTLS) not only radiatively cools the local UTLS region, but also warms the upper stratosphere [12]. The decrease in ODSs concentrations and the subsequent slowdown of ozone depletion caused the flattening of the stratospheric temperature anomalies after 1998 [32,33].

It is important to note that recent observations have shown a significant decrease in lower-stratospheric ozone concentrations in the tropics and Northern Hemisphere (NH) midlatitudes since 1998 due to dynamical variability [34], which cannot be well reproduced by model simulations [35]. Chipperfield found that the linear trends of stratospheric ozone are generally positive in the Southern Hemisphere (SH) and negative in the NH over the past two decades [36]. This interhemispheric difference may lead to an asymmetry of the long-term trends in stratospheric temperature. In this study, we investigate the impact of stratospheric ozone changes on long-term stratospheric cooling in summer and winter in both hemispheres using satellite observations. The effects are further isolated by the stratospheric-ozone-only experiments from the Coupled Model Intercomparison Project Phase-6 (CMIP6).

2. Data and Methods

2.1. Satellite Observations

We use the monthly mean total column ozone from the Multi Sensor Re-analysis version 2 (MSR-2) over 1979–2020 [37,38] with horizontal resolution of $0.5^\circ \times 0.5^\circ$. The MSR-2 is constructed with a data assimilation model using all available satellite observations and surface Brewer and Dobson observations, and is widely used to research the climate impact of ozone variations [11,32]. It is available at <http://www.temis.nl/protocols/O3global.html>, accessed on 15 August 2022.

Monthly mean temperatures in the lower stratosphere (TLS) over 1979–2020 are from the Advanced Microwave Sounding Unit (AMSU) lower stratospheric channel brightness temperature data version 4.0 [39]. The TLS is a combination of MSU channel 4 and AMSU channel 9 with peak sensitivities over approximate range of 150–40 hPa (13–22 km), at a horizontal resolution of $2.5^\circ \times 2.5^\circ$ (data available at <http://www.remss.com/measurements/upper-air-temperature/>, accessed on 13 August 2022).

We use monthly mean middle- and upper-stratospheric temperatures from the merged Stratospheric Sounding Unit (SSU) and AMSU-A observations version 3.0 produced by the National Oceanic and Atmospheric Administration (NOAA) Satellite Applications and Research Center (STAR) [40,41]. SSU is a three-channel infrared radiometer measuring temperatures in the middle and upper stratosphere from 20 to 55 km, with weighting functions that peak at roughly 28, 36 and 45 km, respectively [40]. The dataset was extended from 2006 by mapping the vertical weighting function of the AMSU-A channel onto the weighting function of the SSU channel with a horizontal resolution of $2.5^\circ \times 2.5^\circ$. The merging approach matches weighting functions with high accuracy for SSU channels 1 and 2 and reasonable accuracy for channel 3. The data are available from the NOAA/STAR website (<http://www.star.nesdis.noaa.gov/smcd/emb/mscat/>, accessed on 5 August 2022). Here, we focus on long-term trends December–February (DJF) and June–August (JJA), when ozone variations have the largest influence on the stratospheric temperature.

2.2. Model Simulations

To isolate the impact of ozone variations, we use the stratospheric-ozone-only historical simulations from four CMIP6 models [42–44]. The stratospheric-ozone-only (hist-stratO3) experiments resemble the historical simulations, but are forced by changes in stratospheric ozone concentrations only. There are five CMIP6 models that currently have model outputs of hist-stratO3 simulations. The four models used here are IPSL-CM6A-LR, MIROC6, MRI-ESM2-0, and CanESM5, which have sufficient outputs from 1979 to 2020 available online.

To produce temperature output from the models that is comparable to the satellite datasets, the pressure level output is sampled using the vertical global weighting functions for the three SSU channels (ftp://ftp.star.nesdis.noaa.gov/pub/smcd/emb/mscat/data/SSU/SSU_v3.0, accessed on 22 August 2022) and the TLS channel covering the upper troposphere/lower stratosphere [45]. All the model data are interpolated to a same horizontal grid of CanESM5, and the multi-model ensemble mean is used to calculate the variations in stratospheric temperature.

3. Results

3.1. Long-Term Changes in Stratospheric Ozone

Figure 1 shows the time series of total column ozone anomalies in the period 1979–2020 in the NH and SH. In the NH, ozone depletion in the period 1979–1997 is statistically significant and has comparable magnitudes in JJA and DJF (−6.4 vs. −6.8 DU/decade). After 1998, the ozone trends are still negative but insignificant, because the ozone decrease in the lower stratosphere in the tropics and NH midlatitudes counteracts the ozone recovery in the upper stratosphere. The linear trends during 1998–2020 in boreal summer and winter are −0.7 and −0.3 DU/decade, respectively. In the SH, the ozone depletion during 1979–1997 is stronger than that in the NH, which are −8.9 and −8.0 DU/decade in JJA and DJF, respectively. It is interesting to note that ozone has started to recover since 1998 in the SH, although it is statistically insignificant. The ozone trends in the period 1998–2020 are 0.6 and 1.0 DU/decade in austral winter and summer, respectively.

Figure 2 shows the spatial distributions of total ozone trends over 1979–1997 and 1998–2020 in JJA and DJF. During 1979–1997, ozone trends are significantly negative in most regions (Figure 2a,b). In the NH, the negative trends are mainly located in the middle latitudes with maximum depletion rates of around −16.4 and −26.3 DU/decade in JJA and DJF, respectively. In the SH, the largest ozone reduction occurred over the Antarctic, which can reach about −34.3 and −22.3 DU/decade in JJA and DJF, respectively. During 1998–2020, the magnitudes of the ozone trends are much smaller than those during the period 1979–1997 (Figure 2c,d). It is found that significant ozone recovery occurred in the Antarctic in JJA, with a maximum value of 15.3 DU/decade, which is consistent with the ongoing “healing” of the Antarctic ozone hole after 2000 [46]. In the NH, ozone experienced weak loss in the middle and high latitudes in boreal summer, with a maximum reduction rate of −5.8 DU/decade. However, the ozone depletion is only statistically significant in the east of North America, central Europe, and Greenland. In the SH, positive trends occurred in the middle and high latitudes with a maximum value of 15.3 DU/decade, although the trends are insignificant.

3.2. Long-Term Changes in Stratospheric Temperature

In recent decades, both ozone depletion and increasing GHGs contribute to long-term stratospheric cooling. Ozone absorbs solar ultraviolet radiation and heats the stratosphere. Thus, the cease of stratospheric ozone depletion after 1998 may have important influence on the long-term stratospheric cooling, especially in the summer hemisphere. Figure 3 shows the time series of stratospheric temperature anomalies over the period 1979–2020 in the NH and SH in the three SSU and AMSU channels. Over the ozone-depletion period (1979–1997), stratospheric temperature trends are significantly negative at almost all the altitudes in JJA and DJF. The maximum stratospheric cooling occurs in the uppermost stratosphere (SSU channel 3) and generally decreases with decreasing altitude. It is found

that the magnitude of stratospheric cooling is stronger in summer than in winter, which is likely caused by the ozone depletion. The ozone depletion seems to have stronger influence on the upper and lower stratospheric temperature than in the middle stratosphere. Compared to the cooling in winter, the magnitudes of negative trends in summer in SSU channel 3, 2, 1, and TLS increase by 0.4, 0.4, 0.2, and 0.3 K/decade in the NH, respectively, and 0.5, 0.4, 0.2, and 0.4 K/decade in the SH, respectively. Compared to the trends over 1979–1997, the stratospheric cooling in SSU channel 3, 2, 1, and TLS is reduced by 0.9 (0.6), 0.9 (0.5), 0.7 (0.6), and 0.5 (0.3) K/decade during 1998–2020 in the NH in boreal summer (winter) and 0.7 (0.3), 0.4 (0.1), 0.4 (0.3), and 0.7 (0.1) K/decade during 1998–2020 in the SH in austral summer (winter). It is worth pointing out here that the reduction in the stratospheric cooling is stronger in summer than that in winter, which is caused by the stronger solar radiation and similar ozone depletion in summer relative to that in winter. During 1998–2020, the trends in upper and middle stratospheric temperature are still significantly negative, which indicates the continuous stratospheric cooling mainly induced by the increasing GHGs. In the lower stratosphere, the trends are still negative in both JJA and DJF in the NH, although they are insignificant. In contrast, it shows a small and insignificant warming in austral summer in the SH lower stratosphere with a linear trend of 0.1 K/decade. The lower-stratospheric warming/cooling in summer may be caused by the weak ozone recovery/depletion in the SH/NH.

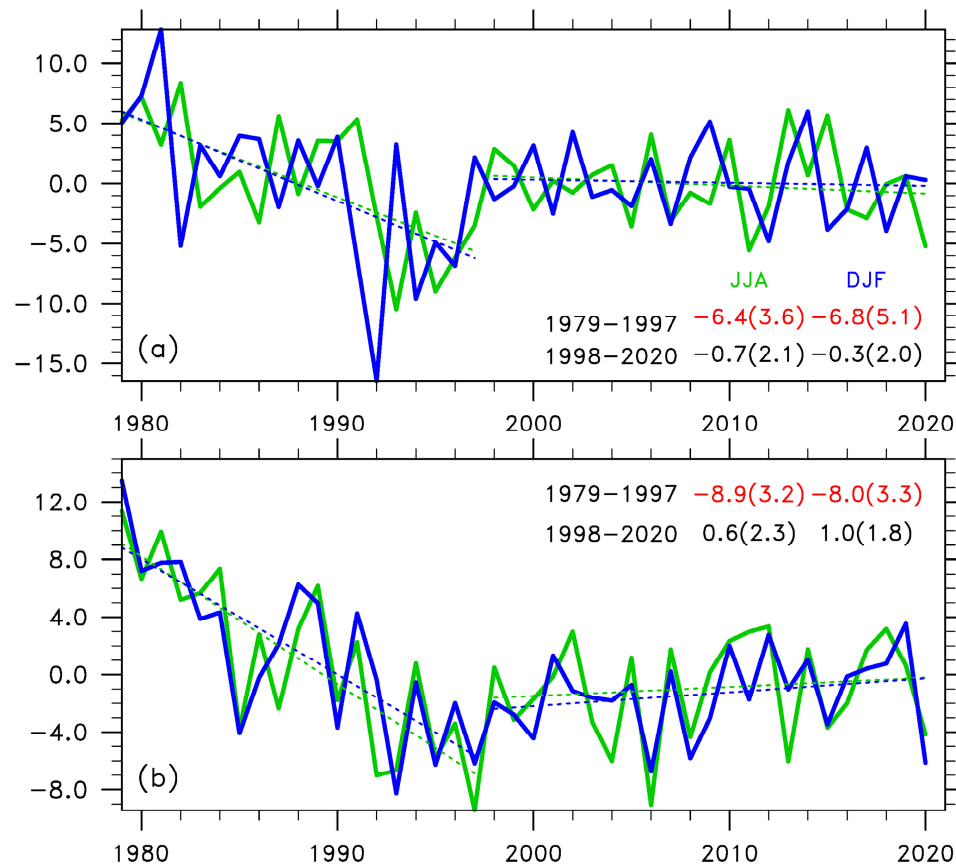


Figure 1. Time series of total column ozone anomalies over 1979–2020 in the (a) NH and (b) SH. The red and blue lines represent total column ozone averaged in JJA and DJF, respectively. The units are Dobson Unit (DU). The dotted lines indicate the linear regression over 1979–1997 and 1998–2020. The linear trends in JJA and DJF over 1979–1997 and 1998–2020 are marked in the upper right of each panel. Red and black values are statistically significant and insignificant, respectively, at the 95% confidence level using Student's t-test, with two σ uncertainties in brackets. The units for the trends are DU/decade.

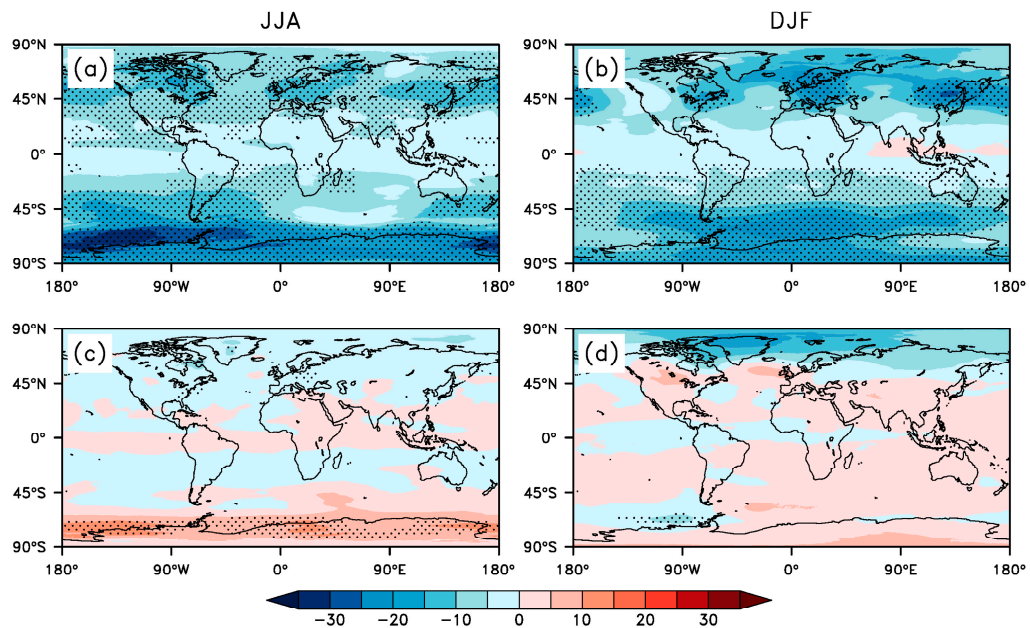


Figure 2. Geographic distributions of linear trends of total column ozone over (a,b) 1979–1997 and (c,d) 1998–2020 in (a,c) JJA and (b,d) DJF. Regions with dots are the places where trends have statistical significance levels higher than the 95% confidence level.

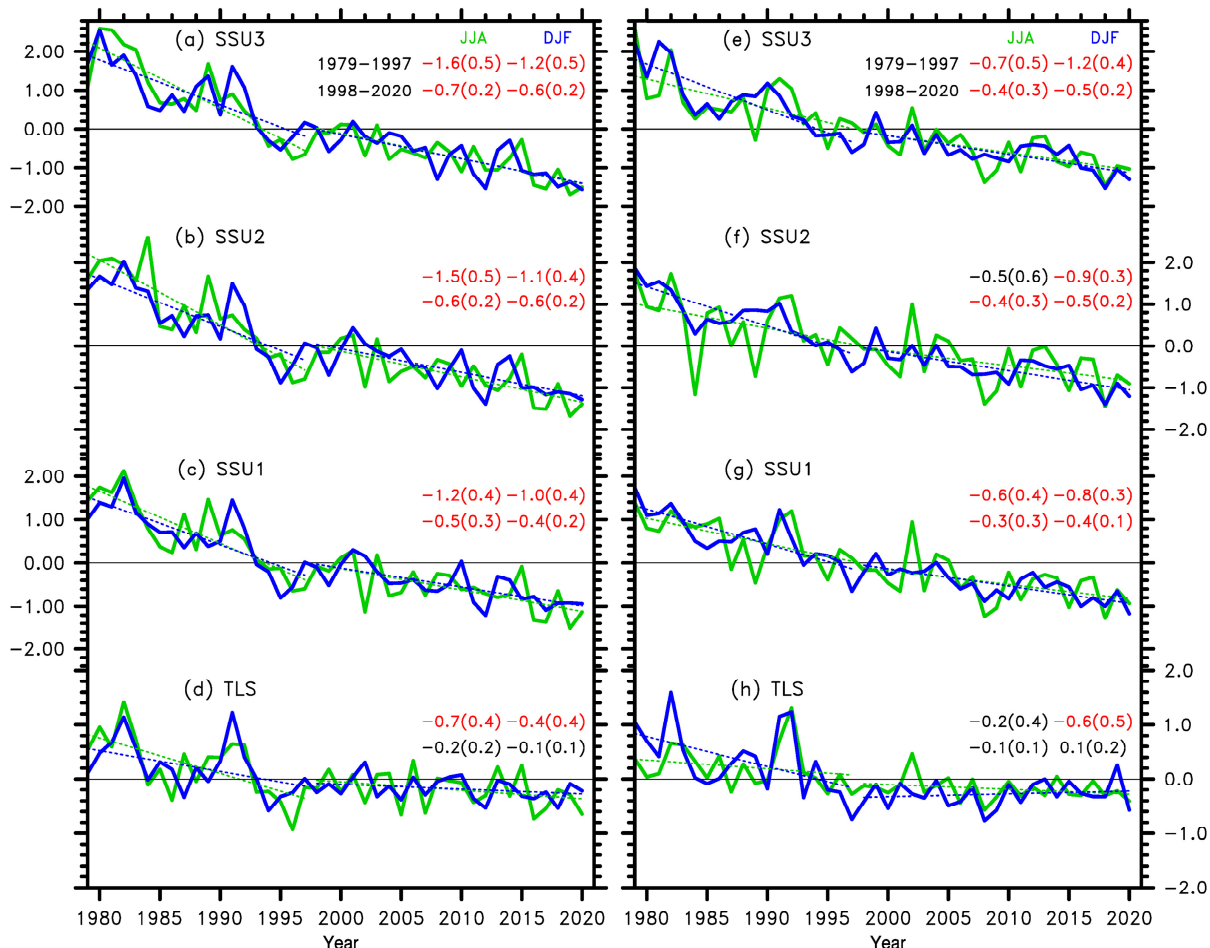


Figure 3. Time series of stratospheric temperature anomalies over 1979–2020 in the (a–d) NH and (e–h) SH in SSU channel (a,e) 3 (~40–50 km), (b,f) 2 (~35–45 km), (c,g) 3 (~25–35 km), and (d,h) TLS. The

green and blue lines represent stratospheric temperature averaged in JJA and DJF, respectively. The units are K. The dotted lines indicate the linear regression over 1979–1997 and 1998–2020. The linear trends in JJA and DJF over 1979–1997 and 1998–2020 are marked in the upper right of each panel. Red and black values are statistically significant and insignificant, respectively, at the 95% confidence level using Student's *t*-test, with two σ uncertainties in brackets. The units for the trends are K/decade

Figure 4 shows the spatial distributions of linear trends in stratospheric temperature over 1979–1997 and 1998–2020 in JJA and DJF in SSU channel 1, 2, 3, and TLS. In SSU channel 3, significant stratospheric cooling occurs in the tropics and summer hemisphere, which can reach -2.9 and -3.2 K/decade over 1979–1997 in JJA and DJF, respectively, and -1.2 and -2.7 K/decade over 1998–2020 in JJA and DJF, respectively (Figure 4a–d). In SSU channel 2 and 1, the maximum cooling is located on the equator and decreases with increasing latitude, except for the high latitudes in the winter hemisphere (Figure 4e–l). In the lower stratosphere, significant cooling mainly occurs in the middle latitudes of the summer hemisphere over 1979–1997, with maximum values of -1.1 and -1.3 K/decade in JJA and DJF, respectively (Figure 4m,n). The long-term trends during 1998–2020 are weak and generally insignificant in the lower stratosphere (Figure 4o,p). Compared to the weak cooling in the NH in boreal summer during 1998–2020, the SH shows a little warming in austral summer, which is consistent with the interhemispheric asymmetry of ozone variations.

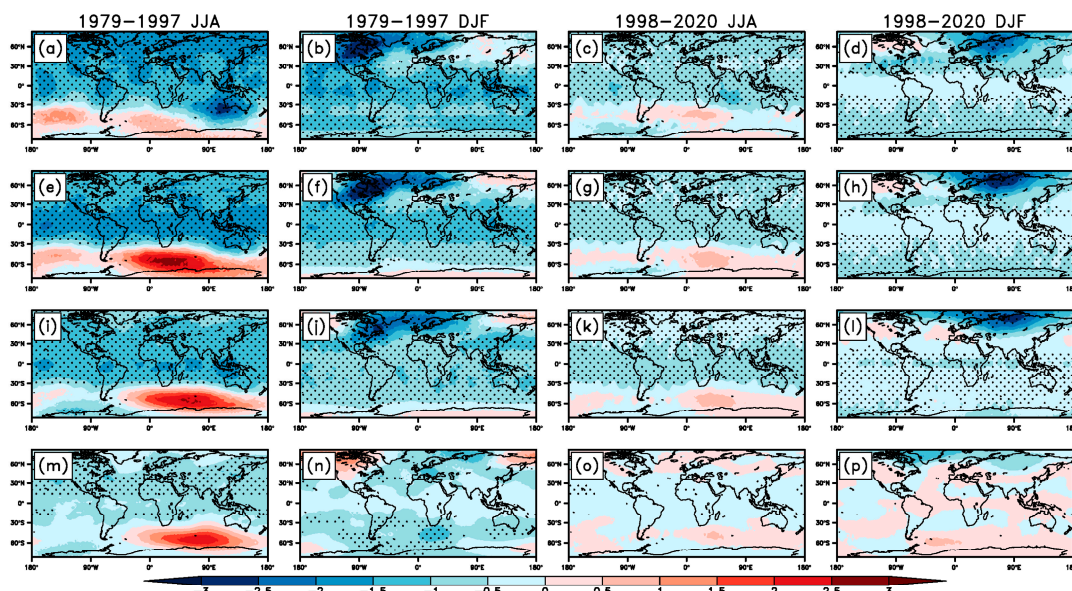


Figure 4. Geographic distributions of linear trends of stratospheric temperature over (left two columns) 1979–1997 and (right two columns) 1998–2020 in JJA and DJF in SSU channel (a–d) 3 (~40–50 km), (e–h) 2 (~35–45 km), (i–l) 1 (~25–35 km), and (m–p) TLS. Regions with dots are the places where trends have statistical significance levels higher than the 95% confidence level.

In the high latitudes of the winter hemisphere, stratospheric temperature is mainly regulated by the dynamical heating associated with the downward branch of the stratospheric Brewer–Dobson Circulation (BDC) [47,48]. In the SH, stratospheric warming is located over the south of Indian Ocean in austral winter over 1979–1997 with maximum values of 1.4 , 3.0 , 2.6 , and 2.5 K/decade in SSU channel 3, 2, 1, and TLS, respectively, which indicates a weakening of the stratospheric polar vortex. These positive values become smaller during 1998–2020, which may be caused by the variations in the planetary wave activities propagating into the stratosphere in the last two decades [32]. In the NH, significant cooling occurs in the middle and upper stratosphere over the Arctic in boreal winter, which exhibits a strengthening of the polar vortex. This cooling, which can reach about -3.3 and -3.1 K/decade in SSU channel 2, is located in North America and Northern Eurasia over

1979–1997 and 1998–2020, respectively, which is consistent with the shift of the Arctic polar vortex towards the Eurasian continent in recent decades [49].

To investigate the long-term trends in the BDC, we define the BDC index as the zonal—mean meridional eddy flux of heat at 100 hPa averaged poleward of 30°N: $[v^*T^*_{100 \text{ hPa}, 30-90^\circ\text{N}/S}]$, where the brackets denote the zonal mean and asterisks denote the deviation from zonal mean following Ueyama and Wallace [50]. Figure 5 shows the time series of the BDC index averaged in winter over 1979–2020 in the (a) NH and (b) SH calculated using ERA5 reanalysis [51]. It is found that the BDC index shows weakly negative trends in the NH in boreal winter. On the contrary, the BDC index is enhanced in austral winter in the SH with linear trends of about 0.3 ± 0.5 and 0.3 ± 0.5 (K m/s)/decade over 1979–1997 and 1998–2020, respectively. This indicates a strengthening of the BDC in the SH, which can well explain the stratospheric warming in the high latitudes of the SH in austral winter, as shown in Figure 4. Nowack indicates that an accelerated BDC associated with global warming leads to a decrease in tropical and subtropical lower stratospheric ozone by bringing more ozone-poor air into the tropical lower stratosphere [52]. The strengthening of the BDC in the SH may result in the decrease in the tropical lower stratospheric ozone, which further enhances the tropical lower stratospheric cooling in austral winter.

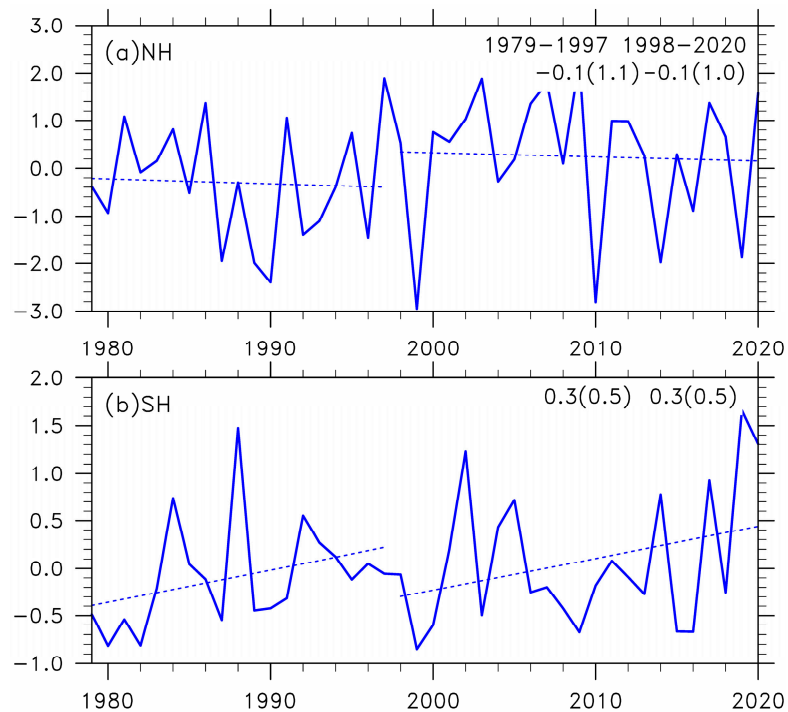


Figure 5. Time series of the BDC index averaged in winter over 1979–2020 in the (a) NH and (b) SH. The units are K m/s . The dotted lines indicate the linear regression over 1979–1997 and 1998–2020. The linear trends over 1979–1997 and 1998–2020 are marked in the upper right of each panel. Red and black values are statistically significant and insignificant, respectively, at the 95% confidence level using the Student's t-test, with two σ uncertainties in brackets. The units for the trends are (K m/s)/decade.

The warming trends in the SH lower stratosphere indicate that ozone recovery likely has a dominant impact on the lower stratospheric temperature in summer over the period 1998–2020. It is found that the correlation coefficients between ozone and stratospheric temperature are larger in summer than that in winter and are the largest in the lower stratosphere in summer, which can reach 0.72 and 0.74 in the NH and SH, respectively (Table 1). Figure 6 shows the spatial distributions of the correlation coefficients between stratospheric temperature and total column ozone over 1979–2020 in JJA and DJF in SSU channel 1, 2, 3, and TLS. In all SSU channels, stratospheric temperature is significantly

correlated with ozone in the middle latitudes of the summer hemisphere. The positive correlation coefficients can reach about 0.74, 0.78, and 0.81 in JJA and 0.76, 0.78, and 0.87 in DJF in SSU channel 3, 2, and 1, respectively. In the lower stratosphere, the correlation coefficients between temperature and ozone are significantly positive over most regions of the world, with maximum values of 0.92 and 0.94 in JJA and DJF, respectively. The correlation analysis suggests that the lower stratospheric temperature is mainly regulated by the ozone variations, especially in the middle latitudes in summer.

Table 1. Correlation coefficients between stratospheric temperature and total column ozone averaged in the NH and SH in JJA and DJF over 1979–2020 in SSU channel 1, 2, 3, and TLS.

		SSU ch.3	SSU ch.2	SSU ch.1	TLS
NH	JJA	0.41	0.40	0.47	0.72
	DJF	0.18	0.16	0.18	0.20
SH	JJA	0.34	0.25	0.36	0.34
	DJF	0.59	0.58	0.66	0.74

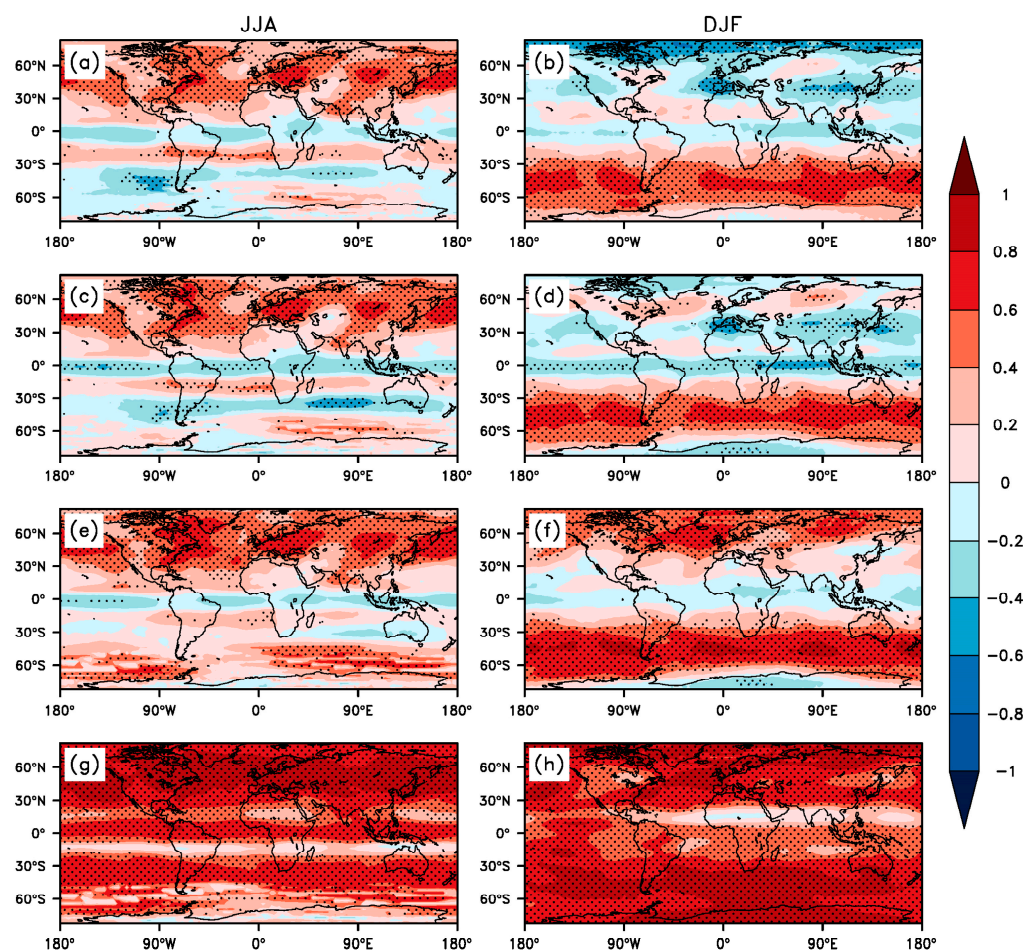


Figure 6. Geographic distributions of the correlation coefficients between stratospheric temperature and total column ozone over 1979–2020 in (a,c,e,g) JJA and (b,d,f,h) DJF in SSU channel (a,b) 3, (c,d) 2, (e,f) 1, and (g,h) TLS. Regions with dots are the places where correlation coefficients have statistical significance levels higher than the 95% confidence level.

3.3. CMIP6 Simulations

The above observational analyses have shown that stratospheric ozone changes play an essential role in the long-term trends of stratospheric temperature. To verify and isolate the impact of stratospheric ozone, we investigate the long-term trends of stratospheric

temperature in response to stratospheric ozone using the ozone-only historical experiment from CMIP6.

Figure 7 shows the time series of multi-model ensemble mean stratospheric temperature anomalies in the NH and SH over 1979–2020 in SSU channel 1, 2, 3, and TLS. During 1979–1997, stratospheric ozone depletion results in significant cooling of the stratosphere, with a stronger negative trend in summer than in winter. The NH temperature trends in boreal summer are -0.47 , -0.33 , -0.27 and -0.26 K/decade in SSU channel 3, 2, 1 and TLS, respectively. In the SH, the stratospheric cooling trends are -0.37 , -0.18 , -0.15 and -0.35 K/decade in austral summer in SSU channel 3, 2, 1 and TLS, respectively. It is found that the ozone-depletion-induced stratospheric cooling is stronger in the upper and lower stratosphere than that in the middle stratosphere in the SH. Compared to the observed trends over 1979–1997, the stratospheric ozone depletion contributes about 29.4% and 37.1% of the upper and lower stratospheric cooling in boreal summer in the NH, respectively. In the SH, about 30.8% and 58.3% of the upper and lower stratospheric cooling can be attributed to the ozone depletion in austral summer, respectively. During 1998–2020, ozone recovery in the upper stratosphere leads to significant warming trends in SSU channel 3, which are about 0.07 and 0.13 K/decade in summer in the NH and SH, respectively. The long-term trends increase by 0.54 (0.48), 0.31 (0.18), 0.21 (0.09), and 0.18 (0.28) K/decade during 1998–2020 compared to that over 1979–1997 in boreal (austral) summer in the NH (SH) in SSU channel 3, 2, 1 and TLS, respectively. The changes in the trends are the strongest in the upper stratosphere, which is consistent with the observations. In the lower stratosphere, the cooling trends are -0.08 and -0.07 K/decade in summer in the NH and SH, respectively, which may be caused by the decrease in lower-stratospheric ozone in tropics in chemistry-climate models [35].

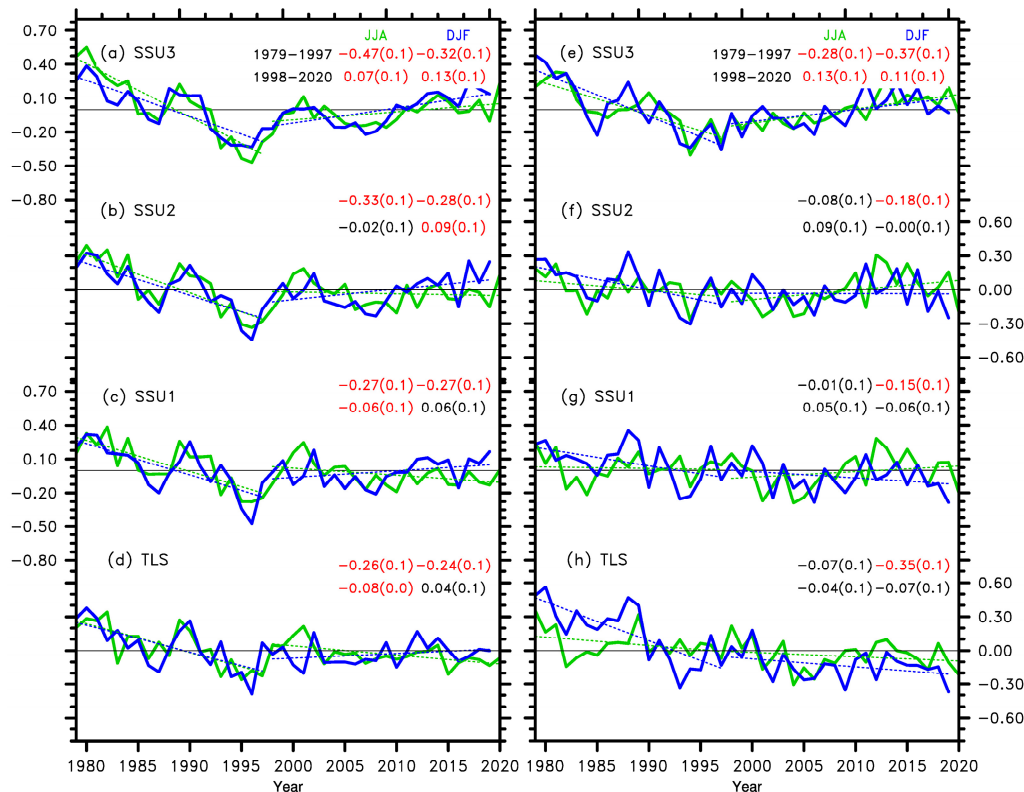


Figure 7. Similar to Figure 3, but for the time series of multi-model ensemble mean stratospheric temperature anomalies over 1979–2020 in the (a–d) NH and (e–h) SH in SSU channel 3 (a,e), 2 (b,f), 1 (c,g), and TLS (d,h).

Figure 8 shows the geographic distributions of multi-model ensemble mean linear trends of stratospheric temperature over 1979–1997 and 1998–2020 in JJA and DJF in SSU

channel 3, 2, 1 and TLS. Over 1979–1997, it is found that significant cooling trends due to ozone depletion mainly occur in the tropics and the summer hemisphere, which is consistent with the observations. The negative trends are stronger in the upper (SSU channel 3) and lower stratosphere than in the middle stratosphere (SSU channel 2 and 1). The maximum cooling trends are -0.57 , -0.42 , -0.40 , and -0.45 K/decade in boreal summer in the NH and -0.60 , -0.28 , -0.31 , and -0.51 K/decade in austral summer in the SH in SSU channel 3, 2, 1 and TLS, respectively. During 1998–2020, ozone recovery leads to significant warming over the summer hemisphere in the upper stratosphere, which can reach about 0.16 and 0.21 K/decade in the NH and SH, respectively. The enhancement of tropical upwelling in the lower stratosphere associated with greenhouse warming results in a decrease in topical ozone and consequent cooling trends over the tropics for TLS, which can reach about -0.28 K/decade. It is important to note that the model simulations cannot reproduce the warming trends in austral summer in the SH, which may be caused by the inconsistency between the simulated and observed ozone trends in the lower stratosphere [35].

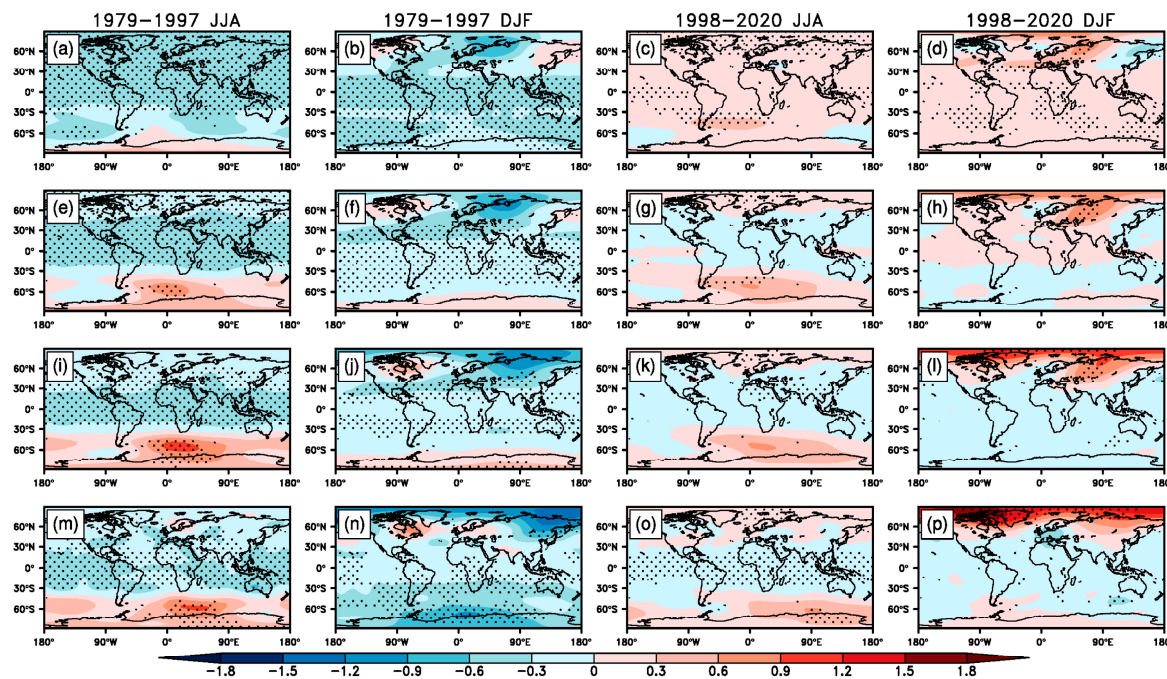


Figure 8. Geographic distributions of multi-model ensemble mean linear trends in stratospheric temperature over (left two columns) 1979–1997 and (right two columns) 1998–2020 in JJA and DJF in SSU channel (a–d) 3, (e–h) 2, (i–l) 1, and (m–p) TLS. Regions with dots are the places where trends have statistical significance levels higher than the 95% confidence level.

The stratospheric ozone variations can impact stratospheric temperature not only via the radiative effects, but also through modifying stratospheric circulation [53,54]. We find that ozone depletion leads to significant warming in the middle and lower stratosphere in austral winter over the Antarctic during 1979–1997, which indicates a strengthening of the Brewer–Dobson Circulation (BDC). Similar results can also be seen in boreal winter over the Arctic during the ozone-recovery period. This ozone-induced warming likely contributes to the Antarctic warming in observations. The wave-mean flow interactions due to stratospheric ozone variations warrant further investigation in future.

4. Conclusions and Discussions

Satellite observations suggest that ozone depletion has been mitigated to varying degrees in both the NH and SH since 1998. We find that ozone experienced little depletion in the NH and weak recovery in the SH over 1998–2020. Further analysis indicates that

the decrease in stratospheric ozone depletion after 1998 has had an important impact on long-term stratospheric cooling, especially in the summer hemisphere. Significant cooling is found to occur in the tropics and summer hemisphere during 1979–1997, which is dramatically reduced over 1998–2020. It is found that the small ozone depletion in the NH led to weak cooling in boreal summer in the NH during the period 1998–2020, while the weak ozone recovery resulted in a warming in austral summer in the SH. The correlation analysis indicates that the lower-stratospheric temperature is primarily regulated by the ozone variations. The stratospheric-ozone-only simulations further isolate the effects of stratospheric ozone and indicate that the ozone recovery during 1998–2020 has caused significant warming in the upper stratosphere in the absence of other factors. The wave-mean flow interactions associated with stratospheric ozone variations may play an important role in regulating the strength of the polar vortex in winter.

Our results indicate that stratospheric ozone variations exert enormous influence on the long-term temperature trends in the stratosphere in recent decades. In observations, the magnitude of the ozone recovery during 1998–2020 is much weaker than that of the ozone depletion during the period 1979–1997. In future, the persistent ozone recovery may counteract the cooling induced by increases in GHGs in the middle and upper stratosphere and lead to warming in the lower stratosphere.

In the last two decades, stratospheric ozone is recovering in the upper stratosphere but decreasing in the lower stratosphere [34]. A previous study has found that ozone variations in the upper troposphere and lower stratosphere can influence temperature in the middle and upper stratosphere by affecting the upward longwave radiation [12].

Thus, the local ozone changes may influence stratospheric temperature at different altitudes. The contributions of ozone changes in different vertical levels to long-term stratospheric temperature trends need further investigation in future.

Author Contributions: Conceptualization, L.Z.; Data curation, Formal analysis, L.Z. and Y.X.; Investigation, Resources, Validation, Visualization, L.Z.; Writing—original draft, Y.X. and C.Z.; Writing—review and editing, Y.X. and C.Z. All authors have read and agreed to the published version of the manuscript.

Funding: This work is supported by the National Natural Science Foundation of China, under grant 42105016, the Second Tibetan Plateau Scientific Expedition and Research Program (STEP), under grant of 2019QZKK0604, Key Laboratory of Middle Atmosphere and Global Environment Observation (LAGEO-2020-09), and the Fundamental Research Funds for the Central Universities. C. Zhao is supported by the National Natural Science Foundation of China, under grant 41925022.

Data Availability Statement: Total column ozone data from MSR-2 is available at <http://www.temis.nl/protocols/O3global.html>, accessed on 15 August 2022. Temperatures in the lower stratosphere (TLS) from the Advanced Microwave Sounding Unit (AMSU) lower stratospheric channel brightness temperature data version 4.0 are available at <http://www.remss.com/measurements/upper-air-temperature/>, accessed on 13 August 2022. Temperatures in middle- and upper-stratospheric are available at <http://www.star.nesdis.noaa.gov/smcd/emb/mscat/>, accessed on 5 August 2022. The vertical global weighting functions for the three SSU channels are available at ftp://ftp.star.nesdis.noaa.gov/pub/smcd/emb/mscat/data/SSU/SSU_v3.0, accessed on 22 August 2022.

Acknowledgments: We thank Jian Yue for helpful comments. We acknowledge the World Climate Research Programme, which, through its Working Group on Coupled Modelling, coordinated and promoted CMIP6. We thank the climate modeling groups for producing and making their model output available, the Earth System Grid Federation (ESGF) for archiving the data and providing access, and the multiple funding agencies who support CMIP6 and ESGF.

Conflicts of Interest: The authors declare no conflict of interest.

References

1. Farman, J.C.; Gardiner, B.G.; Shanklin, J.D. Large Losses of Total Ozone in Antarctica Reveal Seasonal ClO₃NO_x Interaction. *Nature* **1985**, *315*, 207–210. [[CrossRef](#)]
2. Solomon, S. Stratospheric Ozone Depletion: A Review of Concepts and History. *Rev. Geophys.* **1999**, *37*, 275–316. [[CrossRef](#)]

3. Polvani, L.M.; Waugh, D.W.; Correa, G.J.P.; Son, S.-W. Stratospheric Ozone Depletion: The Main Driver of Twentieth-Century Atmospheric Circulation Changes in the Southern Hemisphere. *J. Clim.* **2011**, *24*, 795–812. [[CrossRef](#)]
4. Solomon, S.; Garciat, R.R.; Rowland, F.S.; Wuebbles, D.J. On the Depletion of Antarctic Ozone. *Nature* **1986**, *321*, 755–758. [[CrossRef](#)]
5. Hassler, B.; Young, P.J.; Portmann, R.W.; Bodeker, G.E.; Daniel, J.S.; Rosenlof, K.H.; Solomon, S. Comparison of Three Vertically Resolved Ozone Data Sets: Climatology, Trends and Radiative Forcings. *Atmos. Chem. Phys.* **2013**, *13*, 5533–5550. [[CrossRef](#)]
6. Eyring, V.; Waugh, D.W.; Bodeker, G.E.; Cordero, E.; Akiyoshi, H.; Austin, J.; Beagley, S.R.; Boville, B.A.; Braesicke, P.; Brühl, C.; et al. Multimodel Projections of Stratospheric Ozone in the 21st Century. *J. Geophys. Res. Atmos.* **2007**, *112*, D16. [[CrossRef](#)]
7. Ivy, D.J.; Solomon, S.; Rieder, H.E. Radiative and Dynamical Influences on Polar Stratospheric Temperature Trends. *J. Clim.* **2016**, *29*, 4927–4938. [[CrossRef](#)]
8. Fahey, D.; Newman, P.A.; Pyle, J.A.; Safari, B.; Chipperfield, M.P.; Karoly, D.; Kinnison, D.E.; Ko, M.; Santee, M.; Doherty, S.J. *Scientific Assessment of Ozone Depletion: 2018, Global Ozone Research and Monitoring Project-Report No. 58*; UNEP—UN Environment Programme: Nairobi, Kenya, 2018; p. 591.
9. Xia, Y.; Hu, Y.; Huang, Y. Strong Modification of Stratospheric Ozone Forcing by Cloud and Sea-Ice Adjustments. *Atmos. Chem. Phys.* **2016**, *16*, 7559–7567. [[CrossRef](#)]
10. Xia, Y.; Hu, Y.; Huang, Y.; Bian, J.; Zhao, C. Stratospheric Ozone Loss-Induced Cloud Effects Lead to Less Surface Ultraviolet Radiation over the Siberian Arctic in Spring. *Environ. Res. Lett.* **2021**, *16*, 084057. [[CrossRef](#)]
11. Xia, Y.; Hu, Y.; Huang, Y.; Zhao, C.; Xie, F.; Yang, Y. Significant Contribution of Severe Ozone Loss to the Siberian-Arctic Surface Warming in Spring 2020. *Geophys. Res. Lett.* **2021**, *48*, e2021GL092509. [[CrossRef](#)]
12. Xia, Y.; Huang, Y.; Hu, Y. On the Climate Impacts of Upper Tropospheric and Lower Stratospheric Ozone. *J. Geophys. Res. Atmos.* **2018**, *123*, 730–739. [[CrossRef](#)]
13. Xie, F.; Li, J.; Tian, W.; Fu, Q.; Jin, F.-F.; Hu, Y.; Zhang, J.; Wang, W.; Sun, C.; Feng, J.; et al. A Connection from Arctic Stratospheric Ozone to El Niño-Southern Oscillation. *Environ. Res. Lett.* **2016**, *11*, 124026. [[CrossRef](#)]
14. Xie, F.; Li, J.; Zhang, J.; Tian, W.; Hu, Y.; Zhao, S.; Sun, C.; Ding, R.; Feng, J.; Yang, Y. Variations in North Pacific Sea Surface Temperature Caused by Arctic Stratospheric Ozone Anomalies. *Environ. Res. Lett.* **2017**, *12*, 114023. [[CrossRef](#)]
15. Banerjee, A.; Fyfe, J.C.; Polvani, L.M.; Waugh, D.; Chang, K.-L. A Pause in Southern Hemisphere Circulation Trends Due to the Montreal Protocol. *Nature* **2020**, *579*, 544–548. [[CrossRef](#)] [[PubMed](#)]
16. Harris, N.R.P.; Hassler, B.; Tummon, F.; Bodeker, G.E.; Hubert, D.; Petropavlovskikh, I.; Steinbrecht, W.; Anderson, J.; Bhartia, P.K.; Boone, C.D.; et al. Past Changes in the Vertical Distribution of Ozone—Part 3: Analysis and Interpretation of Trends. *Atmos. Chem. Phys.* **2015**, *15*, 9965–9982. [[CrossRef](#)]
17. Weatherhead, E.C.; Andersen, S.B. The Search for Signs of Recovery of the Ozone Layer. *Nature* **2006**, *441*, 39–45. [[CrossRef](#)] [[PubMed](#)]
18. Bourassa, A.E.; Degenstein, D.A.; Randel, W.J.; Zawodny, J.M.; Kyrölä, E.; McLinden, C.A.; Sioris, C.E.; Roth, C.Z. Trends in Stratospheric Ozone Derived from Merged SAGE II and Odin-OSIRIS Satellite Observations. *Atmos. Chem. Phys.* **2014**, *14*, 6983–6994. [[CrossRef](#)]
19. McLandress, C.; Jonsson, A.I.; Plummer, D.A.; Reader, M.C.; Scinocca, J.F.; Shepherd, T.G. Separating the Dynamical Effects of Climate Change and Ozone Depletion. Part I: Southern Hemisphere Stratosphere. *J. Clim.* **2010**, *23*, 5002–5020. [[CrossRef](#)]
20. Seidel, D.J.; Li, J.; Mears, C.; Moradi, I.; Nash, J.; Randel, W.J.; Saunders, R.; Thompson, D.W.J.; Zou, C.-Z. Stratospheric Temperature Changes during the Satellite Era. *J. Geophys. Res. Atmos.* **2016**, *121*, 664–681. [[CrossRef](#)]
21. De, F.; Forster, P.M.; Shine, K.P. Radiative Forcing and Temperature Trends from Stratospheric Ozone Changes. *J. Geophys. Res. Atmos.* **1997**, *102*, 10841–10855. [[CrossRef](#)]
22. Bohlinger, P.; Sinnhuber, B.-M.; Ruhnke, R.; Kirner, O. Radiative and Dynamical Contributions to Past and Future Arctic Stratospheric Temperature Trends. *Atmos. Chem. Phys.* **2014**, *14*, 1679–1688. [[CrossRef](#)]
23. Fu, Q.; Lin, P.; Solomon, S.; Hartmann, D.L. Observational Evidence of Strengthening of the Brewer-Dobson Circulation since 1980. *J. Geophys. Res. Atmos.* **2015**, *120*, 10–214. [[CrossRef](#)]
24. Mitchell, D.M. Attributing the Forced Components of Observed Stratospheric Temperature Variability to External Drivers. *Q. J. R. Meteorol. Soc.* **2016**, *142*, 1041–1047. [[CrossRef](#)]
25. Austin, J.; Wilson, R.J.; Akiyoshi, H.; Bekki, S.; Butchart, N.; Claud, C.; Fomichev, V.I.; Forster, P.; Garcia, R.R.; Gillett, N.P.; et al. Coupled Chemistry Climate Model Simulations of Stratospheric Temperatures and Their Trends for the Recent Past. *Geophys. Res. Lett.* **2009**, *36*, 13. [[CrossRef](#)]
26. Aquila, V.; Swartz, W.H.; Waugh, D.W.; Colarco, P.R.; Pawson, S.; Polvani, L.M.; Stolarski, R.S. Isolating the Roles of Different Forcing Agents in Global Stratospheric Temperature Changes Using Model Integrations with Incrementally Added Single Forcings. *J. Geophys. Res. Atmos.* **2016**, *121*, 8067–8082. [[CrossRef](#)]

27. Steiner, A.; Ladstädter, F.; Randel, W.; Maycock, A.; Fu, Q.; Claud, C.; Gleisner, H.; Haimberger, L.; Ho, S.-p.; Keckhut, P.; et al. Observed Temperature Changes in the Troposphere and Stratosphere from 1979 to 2018. *J. Clim.* **2020**, *33*, 8165–8194. [CrossRef]
28. Ramaswamy, V.; Schwarzkopf, M.D.; Randel, W.J. Fingerprint of Ozone Depletion in the Spatial and Temporal Pattern of Recent Lower-Stratospheric Cooling. *Nature* **1996**, *382*, 616–618. [CrossRef]
29. Ramaswamy, V.; Chanin, M.-L.; Angell, J.; Barnett, J.; Gaffen, D.; Gelman, M.; Keckhut, P.; Koshelkov, Y.; Labitzke, K.; Lin, J.-J.R.; et al. Stratospheric Temperature Trends: Observations and Model Simulations. *Rev. Geophys.* **2001**, *39*, 71–122. [CrossRef]
30. Son, S.-W.; Gerber, E.P.; Perlitz, J.; Polvani, L.M.; Gillett, N.P.; Seo, K.-H.; Eyring, V.; Shepherd, T.G.; Waugh, D.; Akiyoshi, H.; et al. Impact of Stratospheric Ozone on Southern Hemisphere Circulation Change: A Multimodel Assessment. *J. Geophys. Res. Atmos.* **2010**, *115*, D3. [CrossRef]
31. McLandress, C.; Shepherd, T.G.; Scinocca, J.F.; Plummer, D.A.; Sigmond, M.; Jonsson, A.I.; Reader, M.C. Separating the Dynamical Effects of Climate Change and Ozone Depletion. Part II: Southern Hemisphere Troposphere. *J. Clim.* **2011**, *24*, 1850–1868. [CrossRef]
32. Xia, Y.; Xu, W.; Hu, Y.; Xie, F. Southern-Hemisphere High-Latitude Stratospheric Warming Revisit. *Clim. Dyn.* **2020**, *54*, 1671–1682. [CrossRef]
33. Maycock, A.C.; Randel, W.J.; Steiner, A.K.; Karpechko, A.Y.; Christy, J.; Saunders, R.; Thompson, D.W.J.; Zou, C.; Chrysanthou, A.; Luke Abraham, N.; et al. Revisiting the Mystery of Recent Stratospheric Temperature Trends. *Geophys. Res. Lett.* **2018**, *45*, 9919–9933. [CrossRef] [PubMed]
34. Ball, W.; Alsing, J.; Staehelin, J.; Davis, S.; Froidevaux, L.; Peter, T. Stratospheric Ozone Trends for 1985–2018: Sensitivity to Recent Large Variability. *Atmos. Chem. Phys.* **2019**, *19*, 12731–12748. [CrossRef]
35. Garny, H.; Eichinger, R.; Ball, W. Analysis of Recent Lower-Stratospheric Ozone Trends in Chemistry Climate Models. *Atmos. Chem. Phys.* **2021**, *21*, 6811–6837.
36. Chipperfield, M.; Dhomse, S.; Hossaini, R.; Wuhu, F.; Santee, M.; Weber, M.; Burrows, J.; Wild, J.; Loyola, D.; Coldewey-Egbers, M. On the Cause of Recent Variations in Lower Stratospheric Ozone. *Geophys. Res. Lett.* **2018**, *45*, 5718–5726. [CrossRef]
37. Van der A, R.J.; Allaart, M.A.F.; Eskes, H.J. Extended and Refined Multi Sensor Reanalysis of Total Ozone for the Period 1970–2012. *Atmos. Meas. Tech.* **2015**, *8*, 3021–3035. [CrossRef]
38. Van der A, R.J.; Allaart, M.A.F.; Eskes, H.J. Multi Sensor Reanalysis of Total Ozone. *Atmos. Chem. Phys.* **2010**, *10*, 11277–11294. [CrossRef]
39. Mears, C.; Wentz, F. Construction of the Remote Sensing Systems V3.2 Atmospheric Temperature Records from the MSU and AMSU Microwave Sounders. *J. Atmos. Ocean. Technol.* **2009**, *26*, 1040–1056. [CrossRef]
40. Zou, C.-Z.; Qian, H. Stratospheric Temperature Climate Data Record from Merged SSU and AMSU-A Observations. *J. Atmos. Ocean. Technol.* **2016**, *33*, 1967–1984. [CrossRef]
41. Zou, C.-Z.; Qian, H.; Wang, W.; Wang, L.; Long, C. Recalibration and Merging of SSU Observations for Stratospheric Temperature Trend Studies. *J. Geophys. Res. Atmos.* **2014**, *119*, 13–180. [CrossRef]
42. Meinshausen, M.; Vogel, E.; Nauels, A.; Lorbacher, K.; Meinshausen, N.; Etheridge, D.M.; Fraser, P.J.; Montzka, S.A.; Rayner, P.J.; Trudinger, C.M.; et al. Historical Greenhouse Gas Concentrations for Climate Modelling (CMIP6). *Geosci. Model Dev.* **2017**, *10*, 2057–2116. [CrossRef]
43. Eyring, V.; Bony, S.; Meehl, G.A.; Senior, C.A.; Stevens, B.; Stouffer, R.J.; Taylor, K.E. Overview of the Coupled Model Intercomparison Project Phase 6 (CMIP6) Experimental Design and Organization. *Geosci. Model Dev.* **2016**, *9*, 1937–1958. [CrossRef]
44. Gillett, N.P.; Shiogama, H.; Funke, B.; Hegerl, G.; Knutti, R.; Matthes, K.; Santer, B.D.; Stone, D.; Tebaldi, C. The Detection and Attribution Model Intercomparison Project (DAMIP v1.0) Contribution to CMIP6. *Geosci. Model Dev.* **2016**, *9*, 3685–3697. [CrossRef]
45. Chen, Y.; Han, Y.; Liu, Q.; Delst, P.; Weng, F. Community Radiative Transfer Model for Stratospheric Sounding Unit. *J. Atmos. Ocean. Technol.* **2011**, *28*, 767–778. [CrossRef]
46. Solomon, S.; Ivy, D.J.; Kinnison, D.; Mills, M.J.; Neely, R.R.; Schmidt, A. Emergence of Healing in the Antarctic Ozone Layer. *Science* **2016**, *353*, 269–274. [CrossRef] [PubMed]
47. Hu, Y.; Xia, Y. Extremely Cold and Persistent Stratospheric Arctic Vortex in the Winter of 2010–2011. *Chin. Sci. Bull.* **2013**, *58*, 3155–3160. [CrossRef]
48. Xia, Y.; Hu, Y.; Zhang, J.; Xie, F.; Tian, W. Record Arctic Ozone Loss in Spring 2020 Is Likely Caused by North Pacific Warm Sea Surface Temperature Anomalies. *Adv. Atmos. Sci.* **2021**, *38*, 1723–1736. [CrossRef]
49. Zhang, J.; Tian, W.; Chipperfield, M.P.; Xie, F.; Huang, J. Persistent Shift of the Arctic Polar Vortex towards the Eurasian Continent in Recent Decades. *Nat. Clim. Chang.* **2016**, *6*, 1094–1099. [CrossRef]
50. Ueyama, R.; Wallace, J. To What Extent Does High-Latitude Wave Forcing Drive Tropical Upwelling in the Brewer–Dobson Circulation? *J. Atmos. Sci.* **2010**, *67*, 1232–1246. [CrossRef]
51. Hersbach, H.; Bell, B.; Berrisford, P.; Hirahara, S.; Horányi, A.; Muñoz-Sabater, J.; Nicolas, J.; Peubey, C.; Radu, R.; Schepers, D.; et al. The ERA5 Global Reanalysis. *Q. J. R. Meteorol. Soc.* **2020**, *146*, 1999–2049. [CrossRef]
52. Nowack, P.J.; Luke Abraham, N.; Maycock, A.C.; Braesicke, P.; Gregory, J.M.; Joshi, M.M.; Osprey, A.; Pyle, J.A. A Large Ozone-Circulation Feedback and Its Implications for Global Warming Assessments. *Nat. Clim. Chang.* **2015**, *5*, 41–45. [CrossRef] [PubMed]

53. Zhang, J.; Tian, W.; Xie, F.; Pyle, J.A.; Keeble, J.; Wang, T. The Influence of Zonally Asymmetric Stratospheric Ozone Changes on the Arctic Polar Vortex Shift. *J. Clim.* **2020**, *33*, 4641–4658. [[CrossRef](#)]
54. Hu, Y.; Tung, K.K. Possible Ozone-Induced Long-Term Changes in Planetary Wave Activity in Late Winter. *J. Clim.* **2003**, *16*, 3027–3038. [[CrossRef](#)]